CONTINUUM STRUCTURE IN STRONG ELECTROMAGNETIC FIELDS

Michael O'Connor

Submitted in partial fulfilment of the
requirements for the degree
of
Master of Science
in
Theoretical Physics

University of Cape Town

September 1987

CONTENTS

eigen-value spectra for three super-critical systems is shown below in figure 1.1.

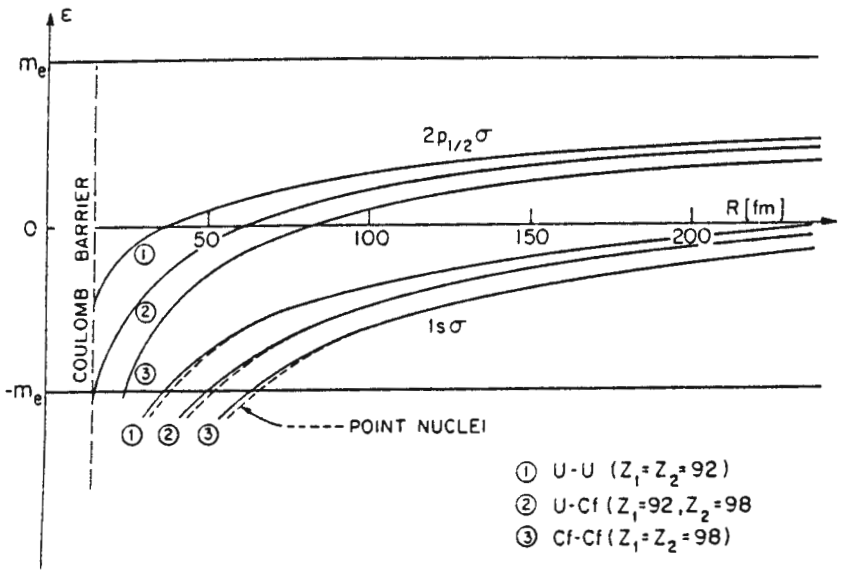

Figure 1.1

The $1s\sigma$ state of the U+U system dives into the lower continuum when R ≈ 30 fm. The lowest Z_u for which this state dives as R approaches the nuclear radius is approximately 178. Ignoring for the moment the time dependence of the collision, one sees that if two U ions are made to just touch, a super-critical field is produced and there is the possibility of the neutral vacuum decaying.

For the ions to just touch, the amount of energy per nucleon required to overcome the Coulomb barrier, C.b., is given by

$$E/A\,\Big|_{C.b.} = Z_1 Z_2 e^2/\mu R_N$$

where μ is the reduced mass and R_N is the nuclear radius. For U on U, this is ~5.7 MeV/A. For a crude estimate of the collision time at the Coulomb barrier, one may use

$$\tau = R_{cr}/v \approx 10^{-21}\,s$$

where R_{cr} is the critical radius (approximately 30 fm) and v is the ion velocity (typically 0.03c to 0.06c).
This is too short by a factor of 100 for one to have any hope of observing the spontaneous vacuum decay. However, it is possible to inrease τ by increasing the energy per nucleon of the ions so that their surfaces

2 The Dirac Equation

2.1 Spherically Symmetric Potentials

In this chapter, the Dirac equation for spherically symmetric potentials is closely examined. Analytical solutions are found for a square well potential, the properties of which will be used later when the equation is solved for arbitrary potentials using numerical methods. The starting point is the Dirac equation for stationary states. For convenience, the units are chosen such that $\hbar$=c=1. However, in explicit calculations, these constants are re-introduced using the prescription $\hbar c$=197 Mev fm. When the coupling constant α is used, its value is taken as 1/137.

$$\left(\alpha\cdot\mathbf{p} + \beta m + V(r)\right)\Psi = E\Psi \tag{2.1}$$

where $V=eA_0$ is the zero component of a 4-vector, $A^{\mu} = (A_0,\mathbf{A})$

In the standard representation,

$$\alpha = \begin{pmatrix} 0 & \sigma \\ \sigma & 0 \end{pmatrix} \qquad \beta = \begin{pmatrix} 1 & 0 \\ 0 & -1 \end{pmatrix} \tag{2.2}$$

Since the potential is spherically symmetric, the angular momentum and parity of the particle are conserved, and the radial dependence of the wavefunction may be separated from the angular dependence.

$$\Psi(r) = \begin{pmatrix} f(r)\chi^{\mu}_{\kappa} \\ ig(r)\chi^{\mu}_{-\kappa} \end{pmatrix} \tag{2.3}$$

where

$\kappa = -\ell-1$ if $j=\ell+\frac{1}{2}$

$\kappa = \ell$ if $j=\ell-\frac{1}{2}$

$$\chi_\kappa^\mu = \sum_m C(\ell\tfrac{1}{2}j;\mu-m,m)Y_\ell^{\mu-m}\chi^m$$

$C(j_1j_2j;m_1m_2m)$ are the Clebsch-Gordan co-efficients, $Y_{\ell,m}$ are the spherical harmonics and χ^m are the two-component spinors.
Using the properties of the Pauli matrices, one obtains

$$\sigma\cdot\mathbf{p} = i(\sigma\cdot\mathbf{r})\left(-\frac{\partial}{\partial r} + \frac{\sigma\cdot\mathbf{L}}{r}\right)$$

χ_κ^μ is an eigenfunction of $\mathbf{J}^2, J_z$ and $\beta(\sigma\cdot\mathbf{L}+1)$ and has the following properties :

$$\mathbf{J}^2\chi_\kappa^\mu = j(j+1)\chi_\kappa^\mu \qquad j_z\chi_\kappa^\mu = \mu\chi_\kappa^\mu$$

$$(\mathbf{L}\cdot\sigma)\chi_\kappa^\mu = -(\kappa+1)\chi_\kappa^\mu \tag{2.4}$$

$$(\sigma\cdot\mathbf{r})\chi_\kappa^\mu = -\chi_{-\kappa}^\mu \tag{2.5}$$

Inserting the ansatz for Ψ into equation (2.1) and using the above properties of χ_κ^μ, one obtains:

$$\begin{pmatrix} m+V(r)-E & i(\sigma\cdot\mathbf{r})(-\frac{\partial}{\partial r} + \frac{\sigma\cdot\mathbf{L}}{r}) \\ i(\sigma\cdot\mathbf{r})(-\frac{\partial}{\partial r} + \frac{\sigma\cdot\mathbf{L}}{r}) & -m+V(r)-E \end{pmatrix} \begin{pmatrix} f\chi_\kappa^\mu \\ ig\chi_{-\kappa}^\mu \end{pmatrix} = 0$$

Multiplying out this equation, and using (2.4) and (2.5), two coupled radial equations are obtained.

$$\left(E-V(r)-m\right)f = -\frac{dg}{dr} + \frac{g(\kappa-1)}{r} \tag{2.6}$$

$$\left(E-V(r)+m\right)g = \frac{df}{dr} + \frac{f(\kappa+1)}{r} \tag{2.7}$$

Differentiating equation (2.7) with respect to r:

Equation (2.11) has the same form as Bessel's modified spherical differential equation, and has the solution[1]

$$f(\lambda r) = Ak_{\ell}(\lambda r) \qquad r>R \tag{2.12}$$

where $\lim_{r\to\infty} k_{\ell}(\lambda r) = \frac{e^{-\lambda r}}{\lambda r}$

In region 1, $V(r)=-V_0$, and $f(r)$ must be regular at the origin.

Write $p^2 = (E+V_0)^2 - m^2$ when $(E+V_0)^2 > m^2$, then (2.12) becomes

$$r^2\frac{d^2f}{dr^2} + 2r\frac{df}{dr} + \left[p^2r^2 - \ell(\ell+1) \right]f = 0 \qquad r\leq R \tag{2.13}$$

(2.13) is the equation satisfied by the spherical Bessel and Neumann functions, and has a solution regular at the origin given by

$$f(pr) = Bj_{\ell}(pr) \qquad r\leq r \tag{2.14}$$

For the case when $(E+V_0)^2 < m^2$, let $(p')^2 = m^2 - (E+V_0)^2$

$$r^2\frac{d^2f}{dr^2} + 2r\frac{df}{dr} - \left[p'^2r^2 + \ell(\ell+1) \right]f = 0 \qquad r\leq R \tag{2.15}$$

The solution to (2.15) which is regular at the origin is

$$f(p'r) = Ci_{\ell}(p'r) \qquad r\leq R \tag{2.16}$$

To determine the functions $g(r)$, use is made of equation (2.7) :

$$g(r) = \left[\frac{df}{dr} + \frac{f(\kappa+1)}{r} \right]/(E+V_0+m) \tag{2.17}$$

Hence, in region 2,

$$g(\lambda r) = \left[\frac{dk_{\ell}(\lambda r)}{dr} + \frac{(\kappa+1)}{r}k_{\ell}(\lambda r) \right]/(E+V_0+m) \tag{2.18}$$

Using the following recurrence relations for Bessel functions, one can find $g(r)$:

$$\frac{dk_n(z)}{dr} = \frac{1}{z}nk_n(z) - k_{n+1}(z)$$

$$\frac{1}{z}(2n+1)k_n(z) = k_{n+1}(z) - k_{n-1}(z)$$

$$\frac{dj_n(z)}{dr} = j_{n-1}(z) - \frac{(n+1)}{z}j_n(z)$$

$$\frac{1}{z}(2n+1)j_n(z) = j_{n-1}(z) + j_{n+1}(z)$$

$$\frac{di_n(z)}{dr} = i_{n-1}(z) - \frac{(n+1)}{z}i_n(z)$$

$$\frac{1}{z}(2n+1)i_n(z) = i_{n-1}(z) - i_{n+1}(z)$$

With the help of these relations, one finds that in region 2,

$$g(\lambda r) = \frac{-A\lambda}{(E+m)} \begin{cases} k_{\ell+1}(\lambda r) & \text{if } \kappa = -\ell-1 \\ k_{\ell-1}(\lambda r) & \text{if } \kappa = \ell \end{cases} \tag{2.19}$$

while in region 1, the two functions g(pr) and g(p′r) are :

$$g(pr) = \frac{Ap}{(E+V_o+m)} \begin{cases} j_{\ell+1}(pr) & \text{if } \kappa = -\ell-1 \\ -j_{\ell-1}(pr) & \text{if } \kappa = \ell \end{cases} \tag{2.20}$$

$$g(p'r) = \frac{Ap'}{(E+V_o+m)} \begin{cases} i_{\ell+1}(p'r) & \text{if } \kappa = -\ell-1 \\ i_{\ell-1}(p'r) & \text{if } \kappa = \ell \end{cases} \tag{2.21}$$

The wavefunction must be continuous at r=R, which implies that

$$\frac{f(pR)}{g(pR)} = \frac{f(\lambda R)}{g(\lambda R)} \tag{2.22}$$

This condition gives the bound state eigenvalues, and is given explicitly for two cases; κ=-1 and κ=+1, these being the s and p states respectively.

In region 2, let $\lambda'^2 = E^2 - m^2$. Equation (2.10) is then

$$r^2\frac{d^2f}{dr^2} + 2r\frac{df}{dr} + \left[\lambda'^2 r^2 - \ell(\ell+1) \right] f = 0 \qquad r>R \tag{2.29}$$

which has the solution

$$f(\lambda' r) = Bj_\ell(\lambda' r) + Cy_\ell(\lambda' r) \qquad r>R \tag{2.30}$$

where $y_\ell(\lambda' r)$ is the spherical Neumann function obeying the same recurrence relations as $j_\ell(pr)$. Hence, the function $g(\lambda' r)$ is

$$g(p'r) = \frac{\lambda'}{(E+V_0+m)} \begin{cases} Bj_{\ell-1}(\lambda' r) + Cy_{\ell-1}(\lambda' r) & \text{if } \kappa=\ell \\ -Bj_{\ell+1}(\lambda' r) - Cy_{\ell+1}(\lambda' r) & \text{if } \kappa=-\ell-1 \end{cases} \tag{2.31}$$

The scattering solutions inside the well are the same as the bound-state solutions given in equations (2.14),(2.16),(2.19) and (2.20). When these are matched to the scattering solutions at r=R, i.e.

$$\frac{f(pR)}{g(pR)} = \frac{f(\lambda' R)}{g(\lambda' R)} \tag{2.32}$$

one of the two constants A and B may be determined. This gives the phase shift experienced by the particle in passing through the potential. Again, for the cases of κ=+1,-1, the matching condition (2.32) is evaluated explicitly here.

Kappa=-1

$$f(\lambda' r) = \left[A\sin(\lambda' r) - B\cos(\lambda' r) \right]/\lambda' r \tag{2.33}$$

$$g(\lambda' r) = \left[\frac{B\lambda' r\sin(\lambda' r) + B\cos(\lambda' r) - A\sin(\lambda' r) + A\lambda' r\cos(\lambda' r)}{(E+m)\lambda'^2 r^2} \right]$$

Before matching (2.33) to (2.23) at r=R, it is convenient to introduce two new quantities, N and δ. Let

$$A = N\cos(\delta) \qquad B = -N\sin(\delta)$$

then (2.33) may be rewritten as

$$f(\lambda' r)=\frac{N\sin(\lambda' r+\delta)}{\lambda' r} \qquad g(\lambda' r)=\frac{\lambda' N}{(E+m)}\left[\frac{\cos(\lambda' r+\delta)}{\lambda' r}-\frac{\sin(\lambda' r+\delta)}{\lambda'^2 r^2}\right] \tag{2.34}$$

Matching equation (2.34) to (2.24) at r=R gives an expression for the phase shift δ.

$$\delta = \arctan\left[\frac{\lambda' R(E+V_0+m)}{(E+m)pR\cot(pR)+V_0}\right]-\lambda' R \qquad \kappa=-1,\ (E+V_0)>m \tag{2.35}$$

$$\delta = \arctan\left[\frac{\lambda' R(E+V_0+m)}{(E+m)p' R\coth(p' R)+V_0}\right]-\lambda' R \qquad \kappa=-1,\ (E+V_0)<m \tag{2.35a}$$

Kappa=+1

$$f(\lambda' r) = A\left[\frac{\sin(\lambda' r)}{\lambda'^2 r^2}-\frac{\cos(\lambda' r)}{\lambda' r}\right]-B\left[\frac{\sin(\lambda' r)}{\lambda' r}-\frac{\cos(\lambda' r)}{\lambda'^2 r^2}\right]$$

$$g(\lambda' r) = \left[\frac{A\sin(\lambda' r)-B\cos(\lambda' r)}{(E+m)r}\right] \tag{2.36}$$

Writing A and B in terms of N and δ, as was done for the κ=-1 state, and matching (2.36) to (2.27):

$$\delta = \arctan\left[\frac{\lambda' R(E+V_0-m)}{(E-m)pR\cot(pR)+V_0}\right]-\lambda' R \qquad \kappa=+1,\ (E+V_0)>m \tag{2.37}$$

$$\delta = \arctan\left[\frac{\lambda' R(E+V_0-m)}{(E-m)p' R\coth(p' R)+V_0}\right]-\lambda' R \qquad \kappa=+1,\ (E+V_0)<m \tag{2.37a}$$

.....

The bound state energy spectrum for a given V_0 and R is obtained by finding the roots of the transcendental equations (2.25) and (2.28) numerically. However, the critical points for κ=-1 where the states dive into the lower continuum may be found analytically by setting E=-m. This yields:

$$\tan\left[(V_0^2-2mV_0)^{\frac{1}{2}}R\right] = 0 \quad \text{or} \quad V_0 = m+\left[n^2\pi^2/R^2+m^2\right]^{\frac{1}{2}}$$

Figure 2.1 below shows a plot of the critical points as a function of V_0 and R, while figure 2.2 shows the bound state spectra for an electron ($m=0.511MeV/c^2$) in a well of radius 200fm. Note particularly that the $\kappa=-1$ state emerges quadratically from the upper continuum and dives linearly into the lower continuum [25], while the $\kappa=+1$ state does the reverse. Figures 2.3 and 2.4 show the phase shifts for those points where the first bound state has E=+m and E=-m. Again, the $\kappa=-1$ states at the upper continuum resemble the $\kappa=+1$ states at the lower continuum. This point is discussed further in chapter 4.

The asymptotic value of the phase shift as $|E| \to \infty$ for the $\kappa=-1$ state is easily found from equation (2.35). As $|E| \to \infty$, $\lambda' \to |E|$ and $p \to |E+V_0|$, and

$$\tan(|E|R+\delta) \to \frac{(E+V_0)|E|R}{E|E+V_0|R\cot(|E+V_0|R)} \qquad \text{as } |E| \to \infty$$

$$\cot(|E|R+\delta) = \cot(|E+V_0|R)$$

$$|E|R+\delta = |E+V_0|R + n\pi$$

$$\delta \to \pm V_0R + n\pi = \mp\int_0^\infty V(r)dr \mp n\pi \qquad \text{as } E \to \pm\infty \qquad (2.38)$$

It can be shown that this condition for the asymptotic phase shift holds for all values of κ, not only the $\kappa=-1$ state for which it was derived above. Equation (2.38) is a statement of **Levinson's Theorem** [12]. The n in the $n\pi$ term counts the number of continuum states pulled down from the upper continuum into the bound state gap, or the number of bound states dragged into lower continuum as the potential strength is increased. The phase shift is usually defined such that $\delta(E=\pm m) = \pm n\pi$ and $\delta(E\to\pm\infty) = \mp\int_0^\infty V(r)dr$. However, since n is not normally known before performing a (numerical) calculation, the phase shift in this work is defined such that $\delta(E=\pm m) = 0$, with the asymptotic phase given by (2.38).

bound state eigenvalues. This is contrary to the rather naive expectation that structure matters in a potential of infinite depth and vanishing range. In the next chapter, an r-dependent potential whose limit as $r \to 0$ resembles a delta function will be discussed. In all respects it closely resembles the square well with $V_0 = \frac{\Omega}{R}$, but the strength parameter Ω for vertical diving in that case is different from $n\pi$.

now the decaying ones, so if the desired solution drifts due to the truncation errors, it is damped back onto its original path.

Let F(r) and G(r) denote the numerical solutions to (2.6) and (2.7), while f(r) and g(r) denote the analytical solutions as before. At r=R, F(R)=f(R) and G(R)=g(R). When the numerical solutions have been advanced to the origin, they can be matched to the analytical square well solutions as was shown previously. Hence, the ratio of F to G at r=0 will equal that of f to g. Define a function y(E) such that

$$y(E)\Big|_{r=0} = \Big(Fg - Gf \Big)_{r=0} \tag{3.3}$$

The roots of y(E) are the required eigenvalues, and are found by solving (3.3) numerically. For the two cases, $\kappa=\pm 1$, the form of y(E) is given.

Kappa=-1

$$F(R) = \frac{e^{-\lambda R}}{\lambda R} \qquad G(R) = \frac{-(1+1/\lambda R)e^{-\lambda R}}{(E+m)R} \tag{3.4}$$

$$y(E) = G(r) + F(r)\left(1-\frac{pr}{\tan(pr)} \right)/(E-V(r)+m)r \qquad E-V(r)>m \tag{3.5}$$

$$y(E) = G(r) + F(r)\left(1-\frac{p'r}{\tanh(p'r)} \right)/(E-V(r)+m)r \qquad E-V(r)<m \tag{3.5a}$$

In order to avoid problems of division by zero in the computer code, the solution is stopped fractionally away from the origin.

Kappa=+1

$$F(R) = \frac{(1+1/\lambda r)e^{-\lambda r}}{\lambda R} \qquad G(R) = -\frac{e^{-\lambda R}}{(E+m)R} \tag{3.6}$$

$$y(E) = F(r) - G(r)\left(1-\frac{pr}{\tan(pr)} \right)\frac{(E-V(r)+m)}{p^2 r} \qquad E-V(r)>m \tag{3.7}$$

$$y(E) = F(r) + G(r)\left(1-\frac{p'r}{\tanh(p'r)} \right)\frac{(E-V(r)+m)}{p'^2 r} \qquad E-V(r)<m \tag{3.7a}$$

$$\delta = \arctan\left[\frac{G(R)\lambda' R}{G(R)-F(R)(E-m)R}\right] - \lambda' R \qquad (3.11)$$

A point to note is that, for small $p'r$, $\frac{\sinh(p'r)}{p'^2r^2}$ and $\frac{\cosh(p'r)}{p'r}$ are large and almost equal numbers, so that care must be exercised when the difference between them is taken, as in (3.8) and (3.10). Since r is very close to zero and p' is small, $p'r$ is small, and a computer will produce nonsense when trying to subtract the two terms. For $p'r<0.3$, the following series expansion is accurate to 10^{-15}, which is the computer accuracy in "double precision." If $p'r>0.3$, the difference between the two terms will be accurate to $\sim 10^{-15}$.

$$\frac{\sinh(x)}{x^2} - \frac{\cosh(x)}{x} \approx \frac{2x}{3!} + \frac{4x^3}{5!} + \frac{6x^5}{7!} + \frac{8x^7}{9!} + \frac{10x^9}{11!} + \frac{12x^{11}}{13!}$$

3.3 The "Discrete" Continuum

One of the objectives of this work is to study the structure of the positive and negative frequency states. However, these are not readily accessable to examination as they stand since there are infinitely many states in any energy interval. If the continuous distribution of states is rendered discrete by some means, the evolution of individual states as some function of the potential may easily be followed, thus giving one some idea of the structure of the "continuum".

Any mathematically consistent boundary condition imposed on the wave-functions at a large value of r will discretise the continuum. In the M.I.T. bag model, quarks are confined to a bag of radius R_0 by introducing a scalar step potential, which leads to the boundary condition:

$$f(R_0) + g(R_0) = 0 \qquad (3.12)$$

where R_0 is the radius of the bag. This condition may be applied without modification to the spherical waves outside the potential well, and leads to an "eigenvalue" equation. Setting f=-g in equations (2.34) and (2.36) immediately gives the "eigenvalue" condition for the $\kappa=\pm 1$ states. These are

3.4 Vacuum Polarisation Charge Density

The charge distribution of the super-critical state (the "charged vacuum") can be calculated using the discrete energy levels found above using a result from quantum field theory, namely:

$$\rho_e(r) = \frac{e}{2} \sum_n \left(\Psi_n^{o\dagger}\Psi_n^o - \Psi_n^{u\dagger}\Psi_n^u \right) - \frac{e}{2} \sum_p \left(\Psi_p^{o\dagger}\Psi_p^o - \Psi_p^{u\dagger}\Psi_p^u \right) \qquad (3.16)$$

Here, $\rho_e(r)$ is the charge density of the dived state, unforunately with the same symbol as that used for the density of states. $\sum_n$ is sum over all levels with E<-m, while $\sum_p$ denotes the sum of all states with E>-m, including bound states. $\Psi^u(r)$ and $\Psi^o(r)$ are the wavefunctions of the under-critical and over-critical states respectively. It is assumed that $\sum_p \left(\Psi_p^{o\dagger}\Psi_p^o - \Psi_p^{u\dagger}\Psi_p^u \right)$ is approximately zero for E>+m when a state dives into the lower continuum, leaving only the bound states in the interval (-m,+m) to be summed in this term. A further assumption made is that the sum $\sum_n \left(\Psi_n^{o\dagger}\Psi_n^o - \Psi_n^{u\dagger}\Psi_n^u \right)$ may be truncated at a finite energy. See figure 3.1.

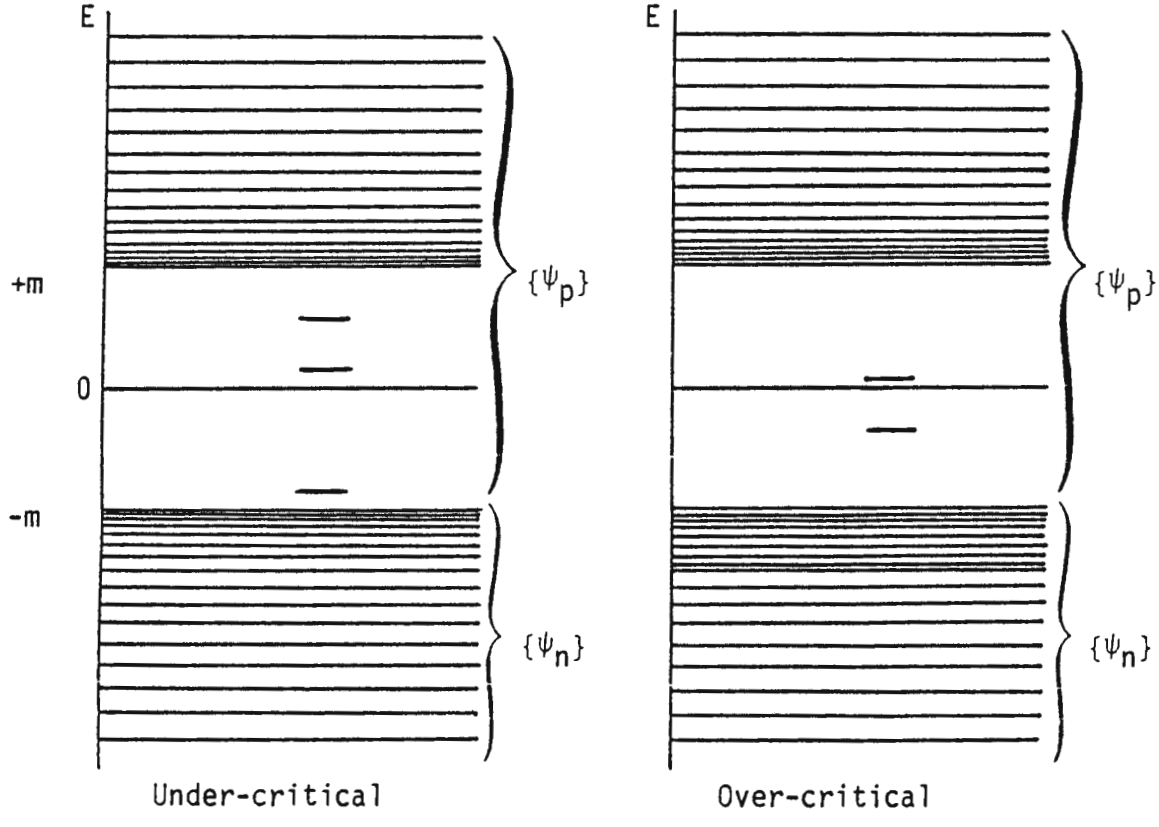

FIGURE 3.1 : $\{\psi_n\}$ and $\{\psi_p\}$ are the sets of negative energy and positive energy states respectively.

Normalised wave functions are required in order to calculate $\rho_e(r)$. The normalisation condition for Dirac wavefunctions, $\int_0^\infty \Psi^\dagger\Psi \, d^3x = 1$, reduces to $\int_0^\infty \left(f^2+g^2 \right) r^2 dr = 1$ in the case of spherical symmetry. Decomposing the integral into the regions inside and outside the well (regions 1 and 2 respectively):

Let $N_1 = \int_0^R \left(f_1^2+g_1^2 \right) r^2 dr$, $N_2 = \int_R^\infty \left(f_2^2+g_2^2 \right) r^2 \, dr$, then $N_1 + N_2 = 1$

N_1 is found by integrating the numerical wavefunctions inside the well using a modified version of Simpson's rule, and N_2 by integrating the analytical expressions for f(r) and g(r) outside the well. The upper limit of integration of ∞ in the expression for N_2 is replaced with the parameter R_0 for the continuum states.

The explicit forms of N_2 follow.

$$N_2 = \frac{(\hbar c)^3 e^{-2\lambda R/\hbar c}}{\lambda^2 (E+m)} \left(\frac{m}{\lambda} + \frac{\hbar c}{(E+m)R} \right) \qquad |E|<m \qquad \kappa=-1 \qquad (3.17)$$

$$N_2 = \frac{(\hbar c)^3 e^{-2\lambda R/\hbar c}}{\lambda^3} \left(\frac{m}{E+m} + \frac{\hbar c}{\lambda R} \right) \qquad |E|<m \qquad \kappa=+1 \qquad (3.18)$$

.....

$$N_2 = \frac{E(R_0-R)(\hbar c)^2}{\lambda'^2 (E+m)} - \frac{m(\hbar c)^3}{2\lambda'^3 (E+m)} \left(\sin 2(\frac{\lambda' R}{\hbar c}+\delta) - \sin 2(\frac{\lambda' R_0}{\hbar c}+\delta) \right) +$$

$$+ \frac{(\hbar c)^4}{\lambda'^2 (E+m)^2} \left(\sin^2(\frac{\lambda' R}{\hbar c}+\delta)/R - \sin^2(\frac{\lambda' R_0}{\hbar c}+\delta)/R_0 \right) \qquad \kappa=-1 \qquad (3.19)$$

$$N_2 = \frac{E(R_0-R)(\hbar c)^2}{\lambda'^2(E+m)} - \frac{m(\hbar c)^3}{2\lambda'^3(E+m)}\left[\sin 2\left(\frac{\lambda' R}{\hbar c}+\delta\right) - \sin 2\left(\frac{\lambda' R_0}{\hbar c}+\delta\right) \right] +$$

$$+ \frac{(\hbar c)^4}{\lambda'^4}\left[\sin^2\left(\frac{\lambda' R}{\hbar c}+\delta\right)/R - \sin^2\left(\frac{\lambda' R_0}{\hbar c}+\delta\right)/R_0 \right] \qquad \kappa=+1 \qquad (3.20)$$

for $|E|>m$.

.....

Before discussing the numerical solutions for more interesting potentials, the square well potential was solved numerically in order to check both the computer programmes and the mathematical basis on which the numerical solutions depend. Using the numerical techniques developed above, the curves shown in figures 2.1 to 2.5 were reproduced. When these were compared to the exact results, a very good agreement was found, with the numerical result differing only in the seventh significant figure in all cases.

4 Short and Long Range Potentials

In this chapter, the behaviour of $s_{\frac{1}{2}}$ states (κ=-1) and $p_{\frac{1}{2}}$ states (κ=+1) under the influence of attractive short range and long range potentials will be examined. It will be shown that, for short range potentials, the positive and negative continua for these two states have a different structure at the points where there are bound states with an energy of E=+m or E=-m. It seems that previously, the $s_{\frac{1}{2}}$ and $p_{\frac{1}{2}}$ continuum states were assumed to have the same structure in a short range potential, in analogy to the Coulomb potential, where they are known to have the same structure.

4.1 The Oscillator Potential

The short range potential under inspection has the form of an oscillator potential.

$$V(r) = -\frac{Ze^2}{2R}\left[3 - \frac{r^2}{R^2} \right] \qquad r<R/3 \qquad (4.1)$$

$$= 0 \qquad r>R/3$$

The reason for choosing this particular form of the potential is that, for r<R, it is the elecrostatic potential inside a uniformly charged sphere, and will be used later as the potential inside a nucleus of radius R. Analytical solutions to the Dirac equation exist for this potential, but these will not be discussed here.

Figure 4.1 shows a plot of the bound states of this potential as a function of Z and R for two different energies, E=+m and E=-m. As in the rest of this work, m is the electron mass and is taken as $0.511 MeV/c^2$.

Since the depth of the potential depends inversely upon R as well as on Z, the potential becomes much like an inverted delta function in the limit as R tends to zero, for a fixed Z. Note that the area under by the potential is $-Z\alpha/3$ and is independent of R. This potential should be compared to the square well with $V_0 = \frac{\Omega}{R}$, which is only slightly

different. The parameter Ω is analagous to the strength $-Z\alpha/3$, and the bound state spectra of these "delta" potentials are similar (see figure 4.1 for the energy spectrum of (4.1) as a function of Z and R). Recall that in the limit as $R \to 0$ for the square well, all energies were allowed when $\Omega=n\pi$, at which point a state dived vertically from the upper to lower continuum. This behaviour is shared by the oscillator potential, with the first two points occuring at Z=268.7 and Z=511.4. The area under the potential for these two values of Z are 1.08π and 2.06π respectively. For the first of these Z values, the bound states are followed to R=0, as shown in figure 4.2. As always, the $s_{\frac{1}{2}}$ state is more bound than the corresponding $p_{\frac{1}{2}}$ state. Both states dive steeply into the lower continuum as R approaches zero.

The bound state energy spectrum is plotted in figure 4.3 as a function of Z for a well with R=100fm (i.e. a range of 100/3fm). Figures 4.4 and 4.5 show the phase shifts at E=+m, where the states emerge from the upper continuum, and at E=-m, where they are absorbed by the lower continuum. These phase shifts should be compared to the similar ones for the square well shown in fig. 2.3 and 2.4. For $\kappa=+1$, the phase jumps down by π when the state is peeled off the upper continuum into the bound state gap, and jumps up by π for $\kappa=-1$ when that state dives into the lower continuum. This is typical of a resonance, where the scattering amplitude, which is proportional to $\sin^2(\delta)$, peaks sharply at some energy. Here, the jump of π over a small energy range ensures that $\sin^2(\delta)$ has a sharp peak.

This is in contrast to the phase of the $\kappa=+1$ state at the lower continuum and that of the $\kappa=-1$ state at the upper continuum. The phase of the $p_{\frac{1}{2}}$ state at E=-m jumps from zero to $-\pi/2$ as Z approaches Z_{cr}, then jumps back to zero for $Z>Z_{cr}$. For E<-m, the phase tends to $-\pi/2$ subcritically then increases to a positive value super-critically. Similarly, the phase of the $s_{\frac{1}{2}}$ state for E>+m tends to zero more and more rapidly as $Z \to Z_{cr}$, has a discontinuity at E=+m of $-\pi/2$ for $Z=Z_{cr}$, then returns to zero at E=+m for Z larger than the critical value. One would not describe these as resonances.

At high energies $|E|>>m$ however, these two cases are very similar in that there is a change of π in the phase when Z increases from below to above the critical value; i.e asymptotically, as $|E| \to \infty$ they are identical.

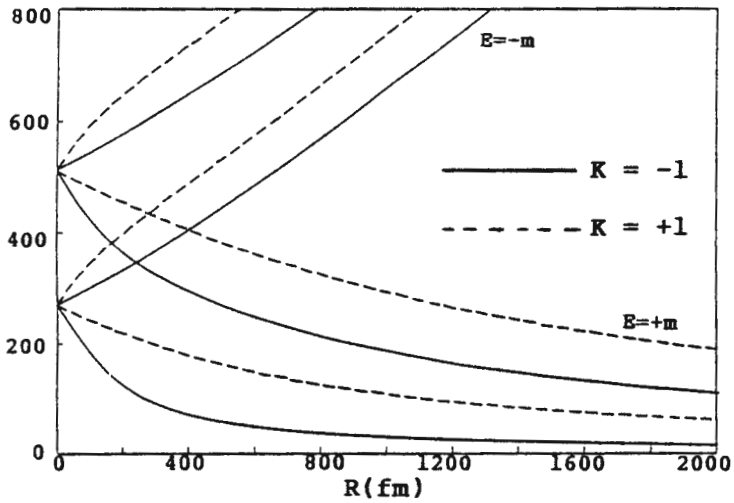

FIGURE 4.1 : Bound states at E = ±M in an oscillator potential as a function of Z and R.

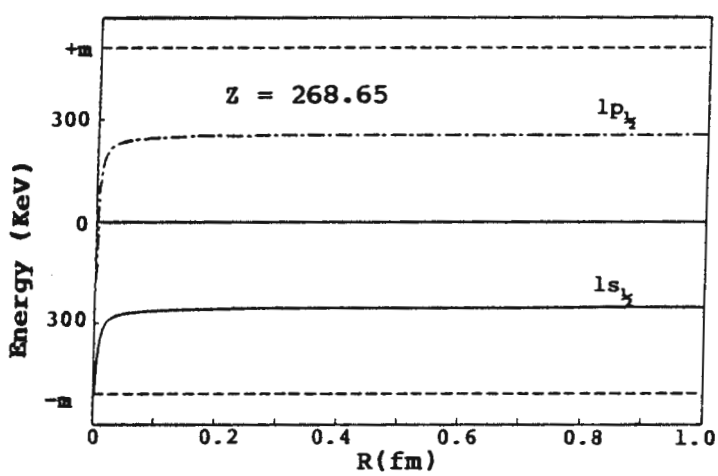

FIGURE 4.2 : Bound states as a function of R.

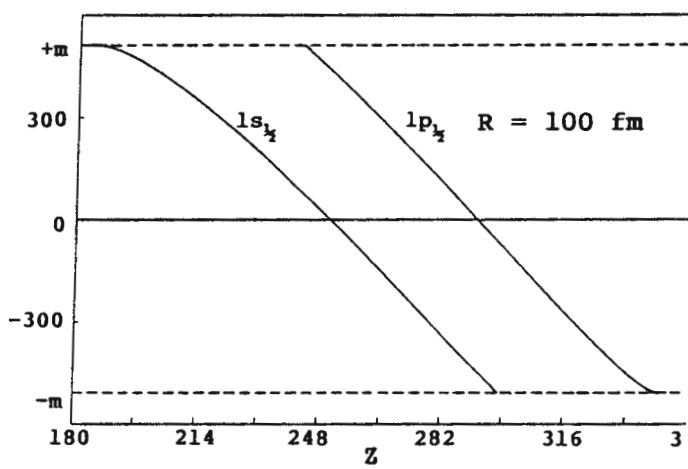

FIGURE 4.3 : Bound states as a function of Z.

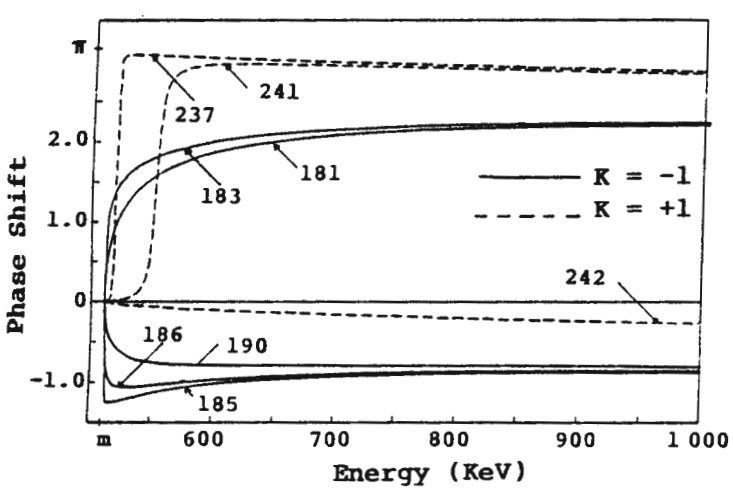

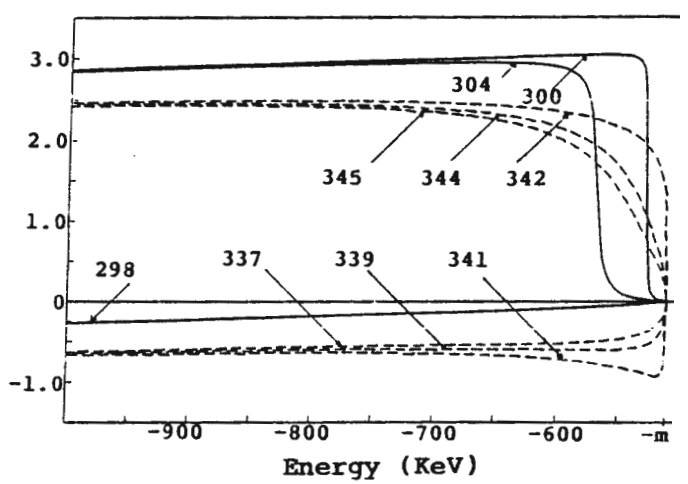

FIGURES 4.4 and 4.5 : Phase shifts in an oscillator potential with R = 100 fm for Z values near the critical points.

The reason for the discontinuity of $\pi/2$ in the phase at $\pm m$ may be found by examining the behaviour of the radial equations (2.6) and (2.7) for $E=+m$, $\kappa=-1$ and $E=-m$, $\kappa=+1$ in region 2 where $V(r)=0$, in conjunction with equations (3.9) and (3.11) for the phase shifts. Recall that the wave function is required to be continuous at $r=R$: $f/g=F/G$. What follows does not apply to long range potentials since there is no region where the potential is zero.

Table 4.1

$E=+m,\ \kappa=-1$	$E=-m,\ \kappa=+1$
$\frac{dg}{dr} = -2\frac{g}{r} \qquad \frac{df}{dr} = -2mg$	$\frac{dg}{dr} = 2mf \qquad \frac{df}{dr} = -2\frac{f}{r}$
$\rightarrow \quad g = Ar^{-2} \qquad f = -A\frac{2m}{r}$	$\rightarrow \quad g = -A\frac{2m}{r} \qquad f = Ar^{-2}$
$\tan(\delta_\kappa) = \frac{F\lambda' R}{2mGR+F} \rightarrow \infty \quad$ as $E\rightarrow m$	$\tan(\delta_\kappa) = \frac{G\lambda' R}{2mFR+G} \rightarrow \infty \quad$ as $E\rightarrow -m$
$\tan(\delta_\kappa) = (n+\frac{1}{2})\pi$	$\tan(\delta_\kappa) = (n+\frac{1}{2})\pi$

These solutions cannot be normalised by $\int_R^\infty \left(f^2+g^2 \right) r^2 dr$ because of the terms containing $1/r$, and are termed "half-bound." It is these "half-bound" states that are responsible for the $\pi/2$ discontinuities observed. The remaining two solutions are not "half bound" and give the phase of π at $\pm m$, as shown below.

Table 4.2

$E=-m,\ \kappa=-1$	$E=+m,\ \kappa=+1$
$\frac{dg}{dr} = -2\frac{g}{r} - 2mf \qquad \frac{df}{dr} = 0$	$\frac{dg}{dr} = 0 \qquad \frac{df}{dr} = -2\frac{f}{r} - 2mg$
$\rightarrow \quad g = Ar^{-2} - \frac{2}{3}mcr \qquad f = c^\dagger$	$\rightarrow \quad g = c^\dagger \qquad f = Ar^{-2} - \frac{2}{3}mcr$
$\tan(\delta_\kappa) = \frac{F\lambda' R}{F} \rightarrow 0 \quad$ as $E\rightarrow -m$	$\tan(\delta_\kappa) = \frac{G\lambda' R}{G} \rightarrow 0 \quad$ as $E\rightarrow m$
$\tan(\delta_\kappa) = n\pi$	$\tan(\delta_\kappa) = n\pi$

†In order to have a normalisable solution, the constant c must be zero. Once again, it should be noted that $\lim_{E\to\pm\infty} \delta(E) = \mp\int_0^\infty V(r)dr \mp n\pi$ where n is the number of states lost by the upper continuum ($E \to +\infty$), or gained by the lower continuum ($E \to -\infty$), in accordance with Levinson's Theorem [12].

The structure of the continua in the region surrounding the dived states can now be examined in terms of the density of states and plots of the discrete energy levels. Figures 4.6a to 4.9a show plots of $\rho(E)-\rho_0(E)$, where $\rho_0(E)$ is the "background" density of states. For $\kappa=-1$, $E\geq m$ and $\kappa=+1$, $E\leq -m$, this "background" is taken as the unperturbed continuum, $\rho_0 \equiv \rho(E)\big|_{V(r)=0}$. It may also be subtracted as the "background" for $\kappa=-1$, $E\leq -m$ and $\kappa=+1$, $E\geq m$ but it is more convenient to use ρ at a sub-critical Z for the former and at a super-critical Z for the latter. The radius of the sphere, R_0, which discretises the continuum has been taken as 10^6 fm. The value of R_0 has no influence at all other than defining how many points there are on these plots since the difference $\rho(E)-\rho_0(E)$ is taken. If R_0 is too small, the points will be widely spaced and fine structure will not be resolved.

Figure 4.6a shows a peak of unit area (one $\kappa=+1$ state) moving down towards $E=+m$ as Z increases, becoming more and more localised in energy as it does so, until it disappears into the gap $(-m,+m)$. The corresponding picture 4.6b illustrates this more explicitly by showing the behaviour of the first few energy levels in the critical region. The first level bends sharply down at Z_{cr} and enters the gap, becoming a bound state, while the next level drops down rapidly to fill its place, shortly followed by the next one up, etc. The splitting between the levels is very small where this rearrangement takes place, so strong coupling between levels can be expected there.

In figure 4.7a for $\kappa=-1$, no highly localised continuum state can be seen diving into the bound state gap: nevertheless, one sees that the continuum is more "dense" relative to the unperturbed continuum for $Z<Z_{cr}$ and less "dense" for $Z>Z_{cr}$. The difference in the integrated density of states between $Z\ll Z_{cr}$ and $Z\gg Z_{cr}$ is just one unit, indicating that the continuum has lost one state. Figure 4.7b shows that this is indeed the case - all the levels in the continuum have moved smoothly down without

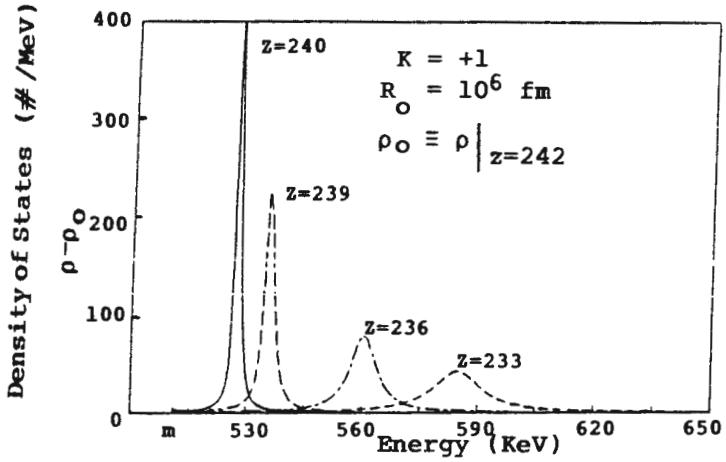

FIGURE 4.6a

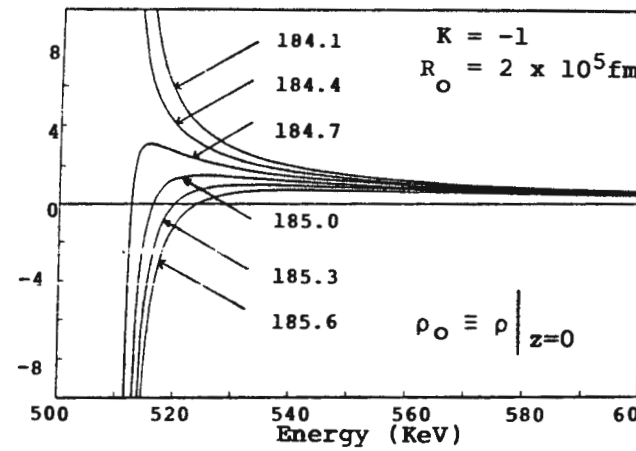

FIGURE 4.7a

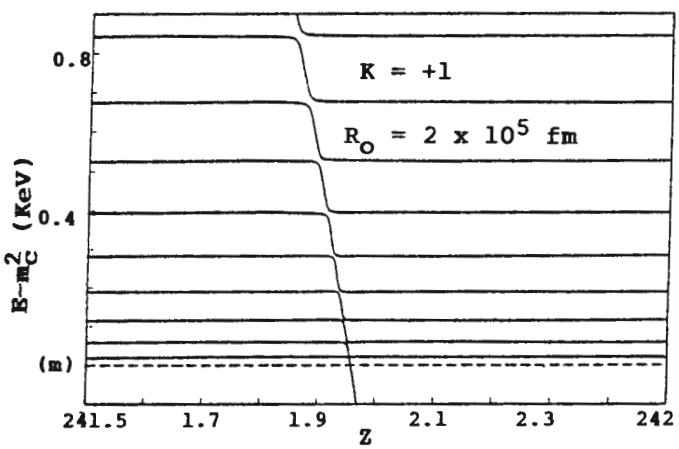

FIGURE 4.6b

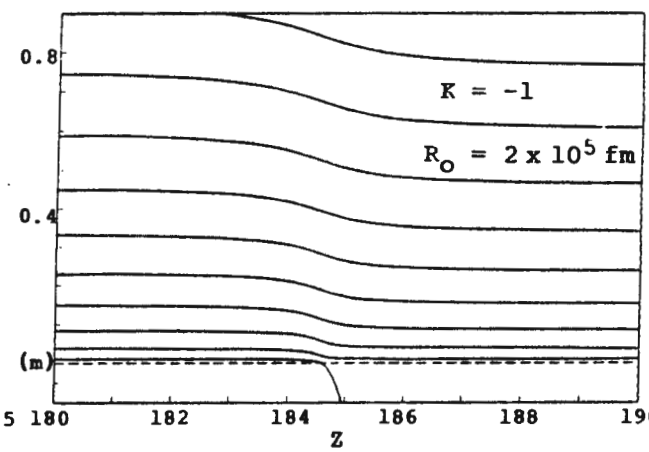

FIGURE 4.7b

LOWER CONTINUUM

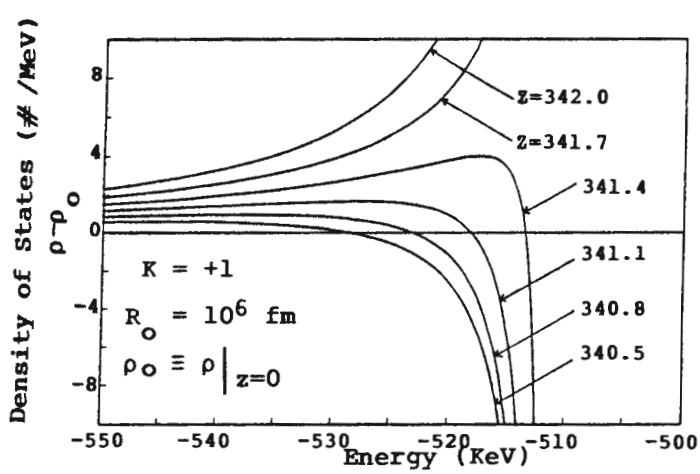

FIGURE 4.8a

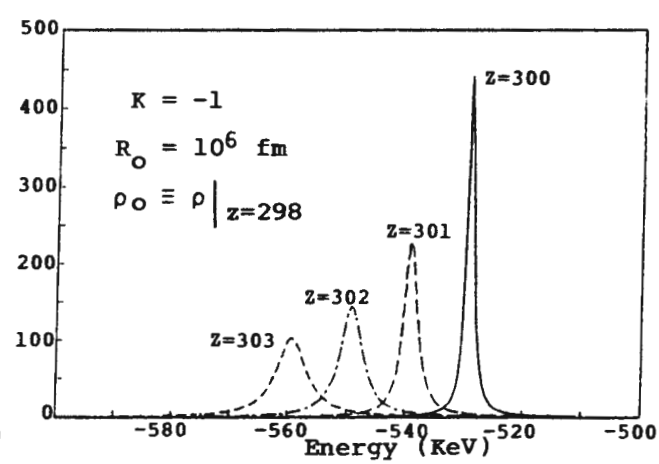

FIGURE 4.9a

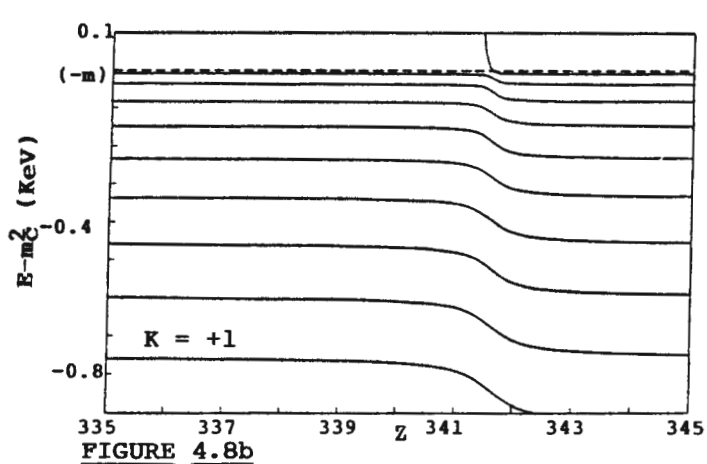

FIGURE 4.8b

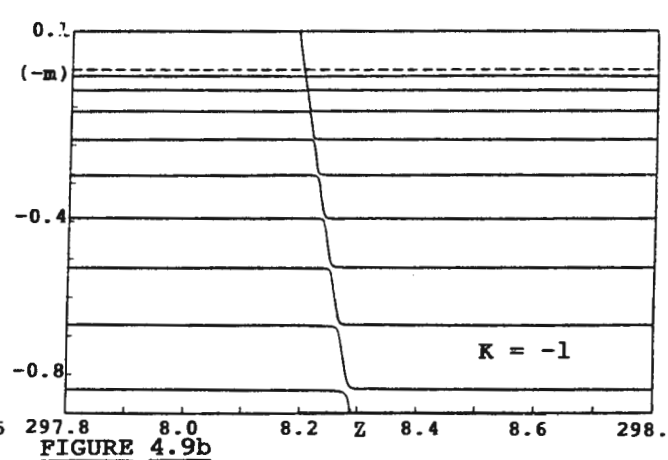

FIGURE 4.9b

changing the spacing between each other, squeezing one level out into the gap.

The situation at the lower continuum is similar, except that now the κ=-1 state is the localised one and the κ=+1 state the diffuse one. The former dives into the lower continuum as a sharp resonance that gradually broadens, while the latter is smoothly incorporated as an extra continuum level. One can say that, because of the strong coupling expected between the levels at the position of the resonance, the former (κ=-1) moves down through continuum, being transmitted from one level to the next. This coupling weakens as the state moves further down into the continuum, until eventually it is dispersed over many energy levels rather than transmitted. In contrast, there is no enhancement at all in the coupling between the κ=+1 continuum states when the bound state reaches E=-m since the spacing betweem levels remains constant. Thus, the bound state is not transmitted down but remains as the first continuum level near E=-m.

Note that the areas quoted on figure 4.9a for the peaks are negative because the ordinate is negative and not because the there is a state missing from the continuum.

The boundary condition, f=-g, on the surface of the sphere at R_0 producing the discrete continuum should not affect the nature of the solutions in the region of the potential. This was checked by arbitrarily changing the boundary condition at r=R_0 to f=+g and re-calculating the discrete continuum levels. The only affect this had was to shift all the energies by a very small constant amount.

4.2 The Damped Coulomb Potential

$$V(r) = -\frac{Ze^2}{2R}\left[3+a - (1+a)\frac{r^2}{R^2} \right] \qquad r<R \qquad (4.2)$$

$$= -\frac{Ze^2}{r} e^{a(1-r/R)} \qquad r>R$$

This is the Coulomb potential for a uniformly charged sphere of radius R, damped by a factor of $e^{a(1-r/R)}$ for r>R. The parameter a determines the amount of damping: for a=0, V(r) reduces to the normal Coulomb potential. Factors of "a" also appear in the oscillator part of the potential so that V(r) and $\frac{dV(r)}{dr}$ match at r=R. The nuclear radius is parametrised by[14]

$$R = 1.2(0.00733Z^2 + 1.3Z + 63.6)^{1/3} \qquad (4.3)$$

which is a good approximation for Z>100.

The potential will not accurately describe the bound states of electrons in light elements with the damping factors which are to be used in this work, since the wave functions of such states are very extended and will be influenced by the "missing" potential in the region where V(r) has been damped to effectively zero. However, near E=m the Coulomb potential is well understood from Schrödinger theory, and is not of interest here. On the other hand, for E≈-m the wavefunctions of bound states are localised in a relatively small region around the origin, so the fact that the potential dies away faster than pure 1/r for large r is immaterial. Hence, to a good approximation, (4.2) will describe the behaviour of electrons in the field of very heavy ions near the lower continuum.

In the previous section, it was seen that κ=-1 and κ=+1 states behaved quite differently at the lower continuum for "short range" potentials. One question to be addressed here is how far does the potential need to extend before the two behave similarly, as they are known to do for a potential of infinte extent. To do this, the parameter "a" will be chosen so that V(r) is effectively zero at a range R_c, so that the effect of the length of the tail, on a potential which is otherwise little different, can be studied. In all that follows, $|V(r)|<10^{-7}$ MeV

will be taken as effectively zero. (This corresponds to $r \approx 2.44\mu m$ for a pure Coulomb potential of Z=170.)

The solid lines on figure 4.10 show the $1s_{\frac{1}{2}}$ and $1p_{\frac{1}{2}}$ bound state spectra as a function of Z, with the potential damped to "zero" at 5×10^{4} fm. The $1s_{\frac{1}{2}}$ state reaches the lower continuum at $Z \approx 171.7$ and the $1p_{\frac{1}{2}}$ state at a Z of about 184.8. With the undamped Coulomb potential, these values are ~173 and ~183 respectively, so this value of the damping factor has little effect near E=-m, as expected. The dashed lines on the figure are the $\kappa=+1$ bound states for different values of the damping constant. The eigen-states near E=+m are much more strongly affected by the change in range of the potential those near E=-m. Examination of the $1p_{\frac{1}{2}}$ and $2p_{\frac{1}{2}}$ bound state wave functions at E=-0.403 MeV and E=0.387 MeV respectively in a well of Z=182 and $R_c=5\times10^{4}$ fm shows clearly the difference in localisation of these states, and why R_c will affect the less bound states more. See figure 4.11c.

The phase shifts in the continuum near the critical Z values in the potential of range 5×10^{4} fm are plotted in figure 4.11b. The phase shift for both the $\kappa=-1$ and the $\kappa=+1$ states show the sudden jump of π which is typical of a resonance. The fairly rapid decrease of δ with E near -m is due to the long range nature of the potential. Recall from equation (4.2) that the asymptotic phase shift for high energies was given by the integral of the potential with respect to r. The integral of (4.3) is

$$\int_0^{R_c} V(r)dr = -Z\alpha e^{a}\left(\frac{4+a}{3}e^{-a} + \ln(B) + \frac{a(1-B)}{1.1!} - \frac{a(1-B^{2})}{2.2!} + \frac{a(1-B^{3})}{3.3!} - \ldots \right)$$

where $B=R_c/R$, and "a" is related to R_c by $a=\ln(R_c\cdot10^{-7}/Ze^{2})/(1-B)$. Although the formula for the asymptotic phase shift is for short range potentials only, it should still hold approximately here since the potential effectively reaches zero. For Z=185 and $R_c=5\times10^{4}$, the value of the integral is -9.3. It is this large value which pulls the phase down.

With a similar phase shift in the region where the states dive, a similar structure in the $s_{\frac{1}{2}}$ and $p_{\frac{1}{2}}$ continua can be expected, and is found. Since the two are so similar, the discretised continuum for the latter only is shown, in figure 4.11a.

STRUCTURE OF THE $1p_{\frac{1}{2}}$ CONTINUUM IN POTENTIALS OF DIFFERENT RANGE

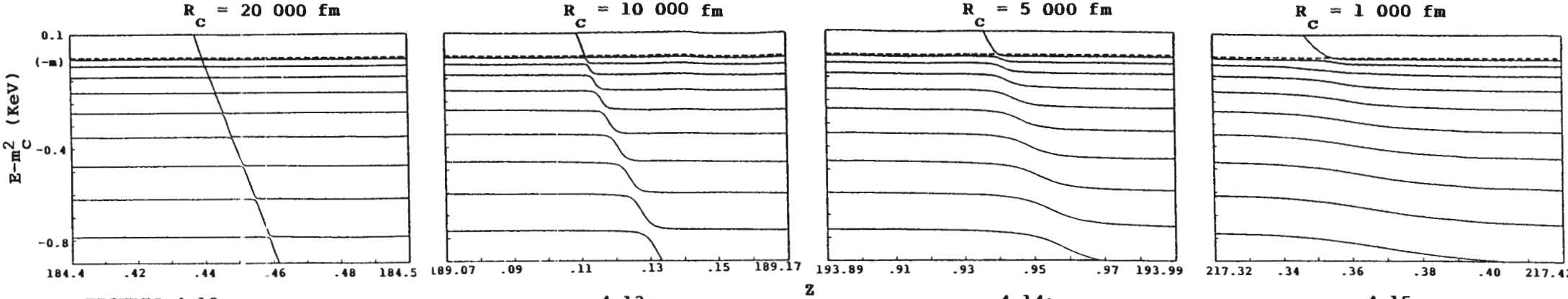

FIGURES 4.12a 4.13a 4.14a 4.15a

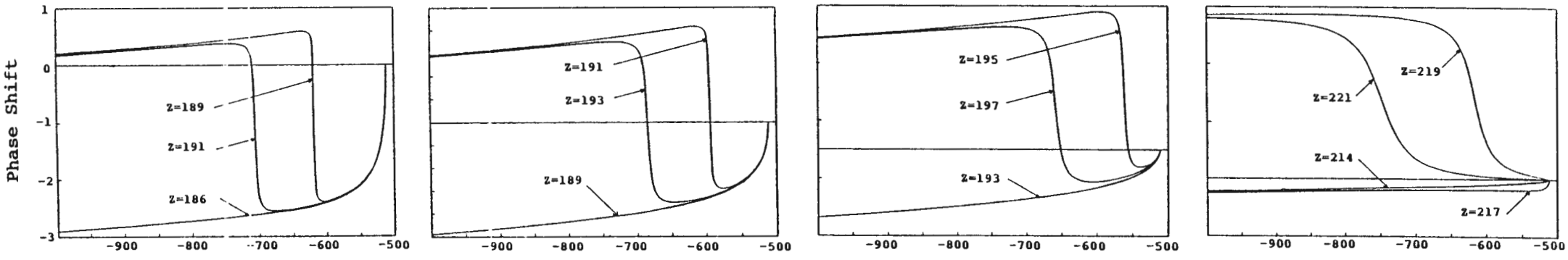

4.12b 4.13b 4.14b 4.15b

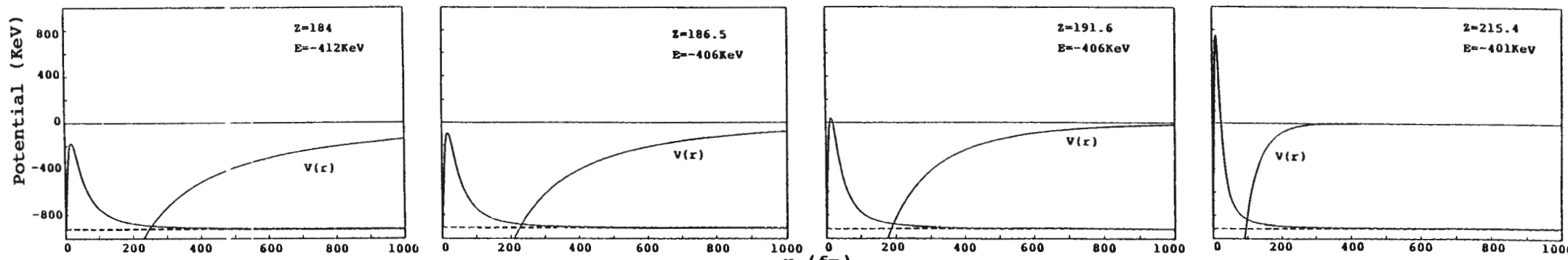

4.12c 4.13c 4.14c 4.15c

The probability density $\psi^{\dagger}\psi^2$ of the $1p_{\frac{1}{2}}$ state is plotted over the potential.

4.3 Charge Distribution of the Super-critical State

Finally, it would be interesting to know if the spatial distribution of the super-critical state differs for short and long range potentials, or if it is different for the $1s_{\frac{1}{2}}$ and $1p_{\frac{1}{2}}$ states in the same potential. Accordingly, the vacuum polarisation charge densities for two different ranges of the damped Coulomb potential are shown for these two states in figure 4.16a.

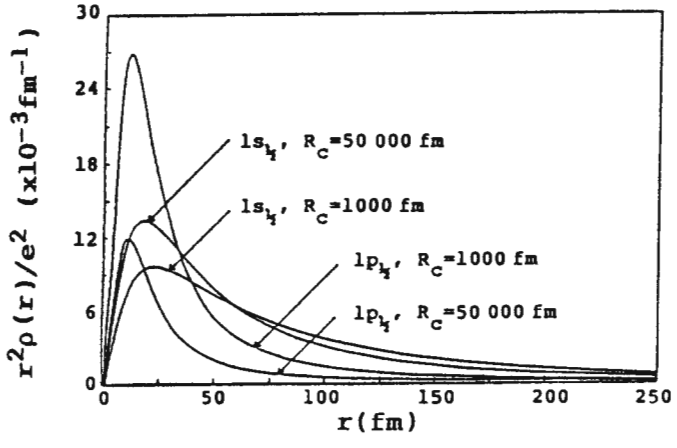

FIGURE 4.16a

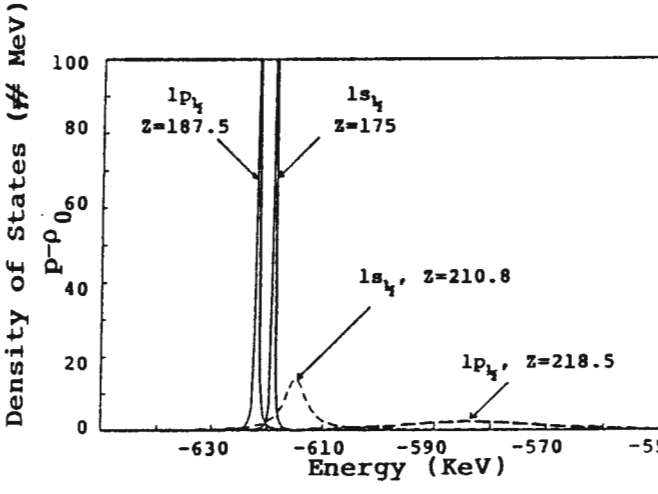

FIGURE 4.16b

As can be seen, changing the range from R_c=1000 fm to R_c=5x10^4 fm does not dramatically change the charge density, nor does it change much from κ=-1 to κ=+1. The charge is localised at between 15 fm and 25 fm from the central charge in all cases, which is just outside the nuclear radius. Figure 4.16b shows the density of the super-critical continuum levels at the Z values for which the charge densities were calculated. The κ=+1 state for R_c=1000 fm is seen to be very broad and flat in comparison with the other three. However, it is still managing to move through the lower continuum, even if it is diffuse, indicating that the potential is still not as "short" as the true short range oscillator potential described earlier. In that potential the state remained at E=-m.

The peak of the vacuum polarisation charge is pulled in towards the central ion as the range is reduced, which is an effect of the increased Z needed to bind the the super-critical state. It is difficult to compare the magnitude of the charge density at the peak of the distribution

5 Potential Models

One of the features a heavy ion collision is the extended region between the ions where the potential is of the order a few MeV (e.g. for a collision between two uranium ions, V≈-1.3 MeV at r=0 when the ions are 400 fm apart). A potential of this depth, extended over a range of the order of the Compton wavelength of the electron, λ_c=386fm, should be able to bind the electron very strongly, and may even produce anomalous structures in the continuum. In this chapter, a spherically symmetric potential is invented to model this feature of the two-centre potential. It will be used to examine the continuum for any "exotic" effects that it may produce.

5.1 A Three-Dimensional Shell Potential

$$V_1(r) = -\frac{Ze^2}{2R_N}\left[\, 3+a - (1+a)\frac{(r+R)^2}{R_N^2} \,\right] \qquad r+R<R_N \qquad (5.1)$$

$$= -\frac{Ze^2}{r+R}\, e^{a(1-(r+R)/R_N)} \qquad r+R>R_N$$

$$V_2(r) = -\frac{Ze^2}{2R_N}\left[\, 3+a - (1+a)\frac{(r-R)^2}{R_N^2} \,\right] \qquad |r-R|<R_N \qquad (5.2)$$

$$= -\frac{Ze^2}{|r-R|}\, e^{a(1-|r-R|/R_N)} \qquad |r-R|>R_N$$

$$V(r) = V_1(r) + V_2(r) \qquad (5.3)$$

R_N is the nuclear radius, with the same parametrisation given in equation (4.4).

For R=0, V(r) is basically the damped Coulomb potential of the previous chapter. However, the charge of the nucleus is then 2Z while R_N is the radius of a nucleus of charge Z. When the parameter R is increased, the

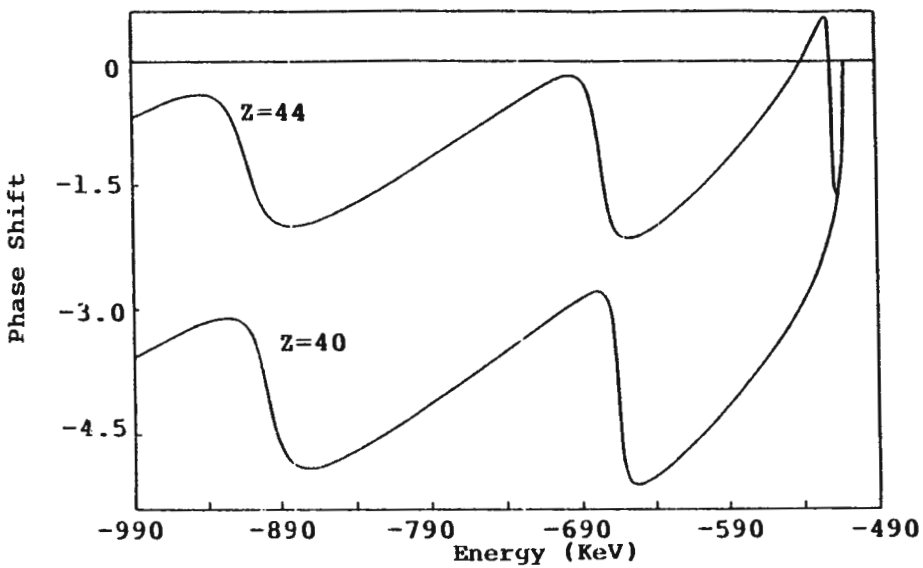

FIGURE 5.5a :

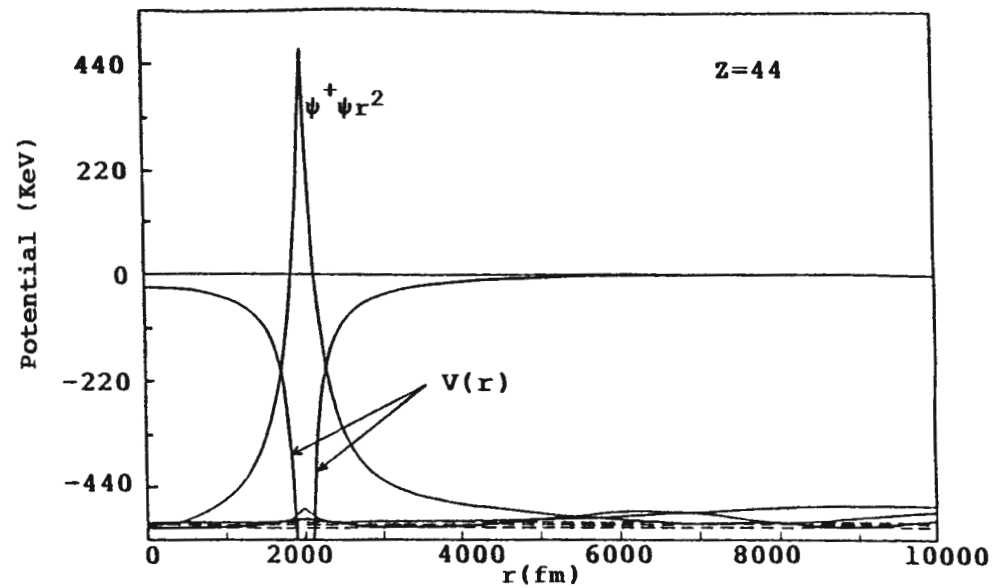

FIGURE 5.5b

Phase shift and wavefunctions of the $1p_{\frac{1}{2}}$ state in a "shell" potential with R = 2000 fm.

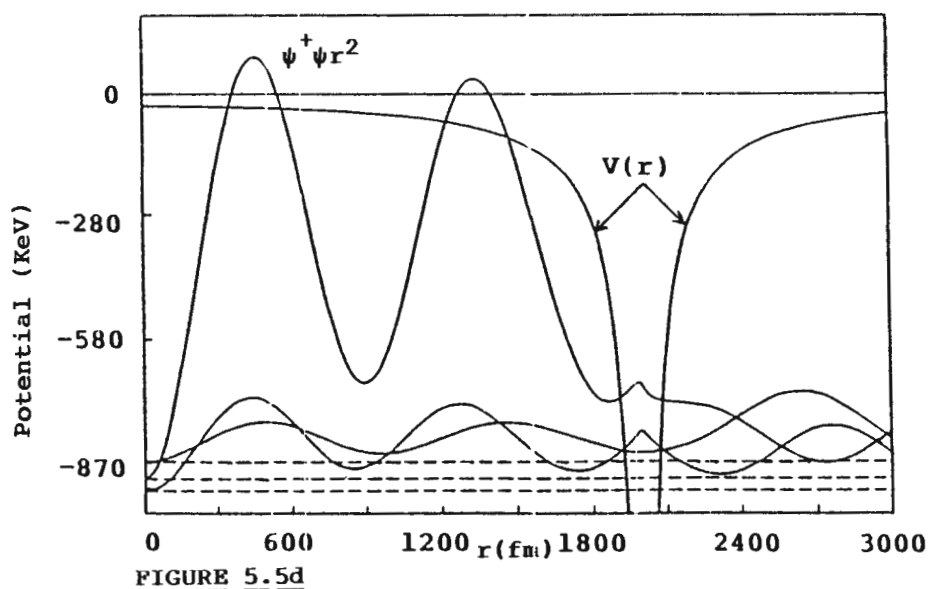

FIGURE 5.5d

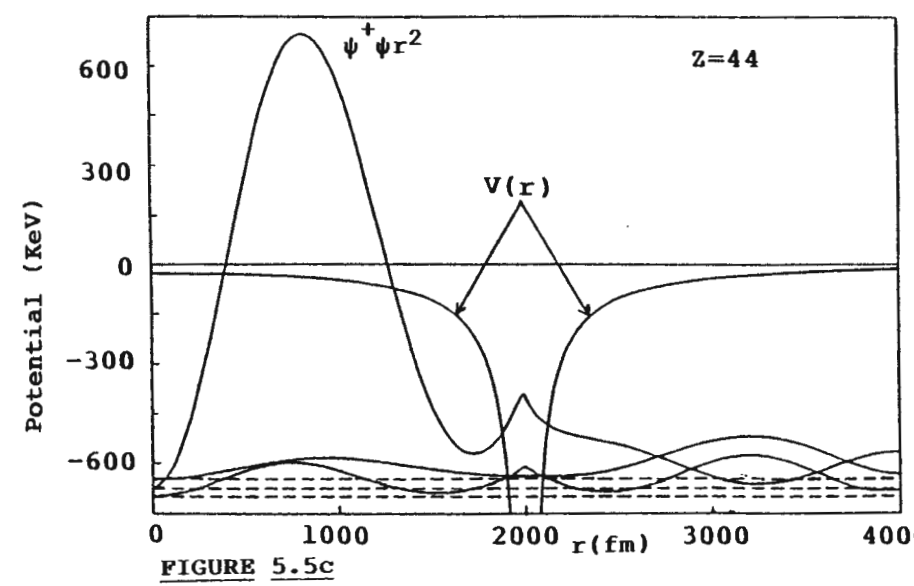

FIGURE 5.5c

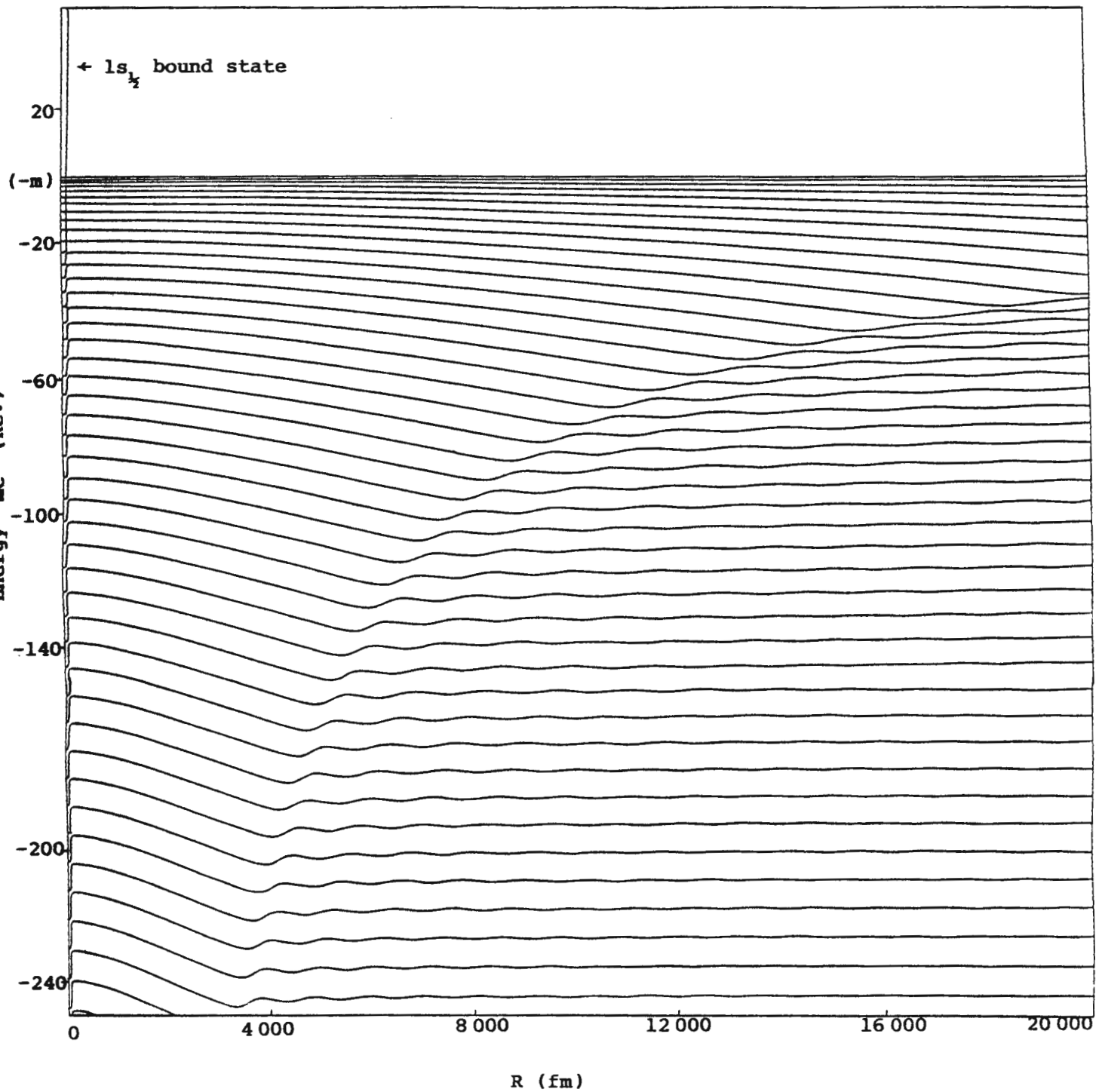

FIGURE : 5.8 The structure of the lower continuum in a square well potential with $V_o = \frac{\Omega}{R} = 3.41$.

6 Conclusion

A framework was devised for obtaining numerically the bound state and continuum solutions for Dirac particles moving in arbitrary vector potentials. By enclosing the potential and particles in a large sphere of radius R_0, the energies of the scattering states were discretised, allowing their evolution as some function of the potential to be studied. This proved to be a very helpful tool in understanding the structure of the continuum, and could also be applied in other areas of physics.

A difference in continuum structure between short and long range potentials was found for the $s_{\frac{1}{2}}$ and $p_{\frac{1}{2}}$ states. In a sufficiently strong long range potential, both the $s_{\frac{1}{2}}$ and $p_{\frac{1}{2}}$ states dived into the lower continuum, while only the $s_{\frac{1}{2}}$ state dived in a short range potential. For the latter potential, the $p_{\frac{1}{2}}$ state resembled the $s_{\frac{1}{2}}$ state with the sign of the energy reversed. It was found that a potential is "long" range if the bound state wave-function of the particle dies within that range, and "short" range if it still has an appreciable probability of being found outside the range.

Many resonances were found in the phase shifts of the scattering states; resonances which were not associated with the diving of a bound state. It would be of interest to examine these resonances more closely than was done in this work, to see what, if any, their consequences are in terms of particle pair production, and if they can shape the energy spectra of free pairs in the vacuum. Further potentials, in particular the two centre Coulomb potential, could be examined to see if such resonances occur there.

[23] G.A.Rinker and L.Wilets: Phys. Rev. **A12**, 748 (1975)

[24] M.E.Rose: Relativistic Electron Theory (Wiley, New York 1961)

[25] P.Seba: Laboratory of Theoretical Physics, Joint Institute for Nuclear Research, 141 980 Dubna, USSR, "On the Absorption of Eigenvalues by Continuous Spectrum in the One and Three Dimensional Dirac Equation". To be published.

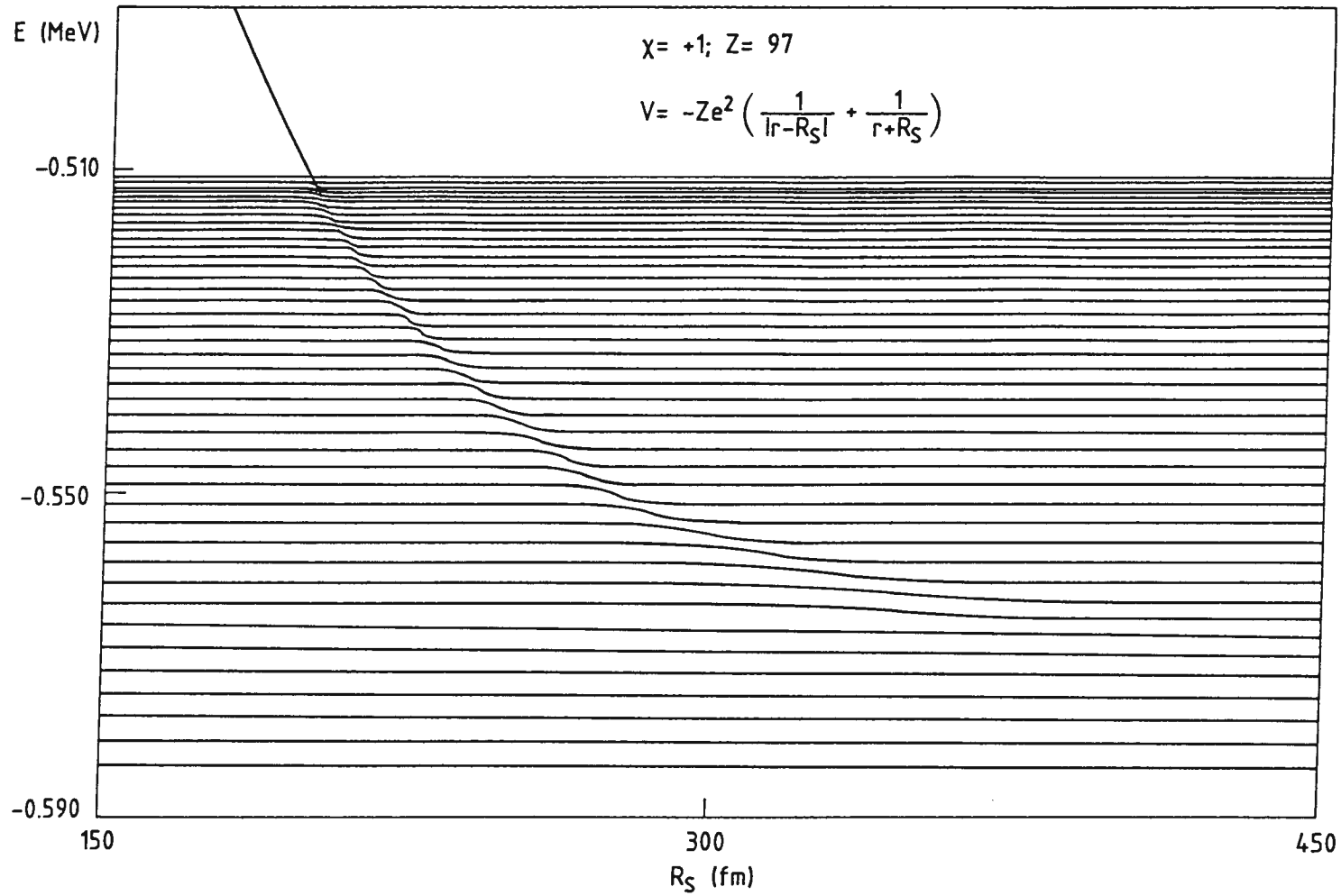

Illustration of the $1p_{\frac{1}{2}}$ state diving into the lower continuum in a "Shell" potential